Electronic properties and valence state of Sm in $(SmS)_{1.19}TaS_2$

Kazuya Suzuki and Toshiaki Enoki
Department of Chemistry, Faculty of Science, Tokyo Institute of Technology, 2-12-1 Ookayama, Meguro-ku, Tokyo 152, Japan

Shunji Bandow
Institute for Molecular Science, Myodaiji, Okazaki 444, Japan
(Received 14 May 1993)

We have investigated the valence state of Sm in $(SmS)_{1.19}TaS_2$, which has an alternate stacking of SmS and TaS_2 layers, by means of electrical transport, magnetic, and x-ray photoemission spectroscopy (XPS) measurements. The transport properties of $(SmS)_{1.19}TaS_2$ are quite similar to those of other analogs $(RS)_xTaS_2$ with a trivalent rare-earth element R, suggesting that the predominant conduction carriers are on the TaS_2 layers. On the contrary the magnetic susceptibility is not explained simply in terms of the trivalent Sm with Curie-Weiss behavior. The Sm 3*d* core-level XPS spectra of $(SmS)_{1.19}TaS_2$ exhibit two sets of peaks associated with both divalent and trivalent Sm initial states, and the portion of Sm^{2+} is estimated at 0.12. Taking into consideration the conduction mechanism and the charge-transfer rate from SmS to TaS_2, it is concluded that the Sm^{2+}-Sm^{3+} valence fluctuation is realized in $(SmS)_{1.19}TaS_2$. We also propose that carriers are localized on the SmS layer due to the quasiperiodic potential.

I. INTRODUCTION

Ternary sulfides $(RS)_xTaS_2$ (R is a rare-earth metal; $x=1.13-1.23$) have a unique crystal structure consisting of the alternate stacking of RS and TaS_2 layers, where RS forms a double layer with pseudotetragonal symmetry and TaS_2 forms a sandwiched layer with pseudohexagonal symmetry.[1,2] Since the crystal symmetries are different between these two kinds of layers, $(RS)_xTaS_2$ exhibits structural incommensurability in an in-plane direction. The lattice constant of pristine RS (NaCl-type cubic symmetry) ranges from 5.75 to 5.61 Å depending on the atomic number of R, while the in-plane lattice parameter of pristine TaS_2 (hexagonal symmetry) is 3.31 Å. If the unit cell of the TaS_2 sublattice is taken as orthohexagonal, the in-plane lattice parameters become 5.73 and 3.31 Å. Since the lattice parameter of the longer axis of the orthohexagonal unit cell is close to the lattice parameter of RS, the sublattices of RS and TaS_2 layers in $(RS)_xTaS_2$ are adjusted in one in-plane direction (crystallographic b axis) with a common lattice parameter. On the other hand, the lattice parameters in the other direction (a axis) take independent values to minimize the change in the cell volume of each layer when the alternate stacking is formed. Then the ratio of the lattice parameter becomes irrational and their lattices become incommensurate; the unit cells are no longer common between the two layers. The chemical composition x in $(RS)_xTaS_2$ is calculated from the ratio of the lattice parameters in the incommensurate direction, so that x also becomes irrational ranging from 1.13 to 1.23 with increasing atomic number of R.[3] The incommensurability, including the irrational ratio of the chemical composition, plays an essential role in the structural and physical properties of $(RS)_xTaS_2$.

Such lattice incommensurability reflects the weak coupling between RS and TaS_2 layers, so that the strong anisotropy is expected in the physical properties of $(RS)_xTaS_2$. (RS_xTaS_2 is a magnetic system which consists of a unit of magnetic double layers inserted into the TaS_2 metallic host. The RS layers have a more two-dimensional nature than other intercalation compounds because of weak interlayer coupling. In addition, the double layer structure of RS can introduce a three-dimensional perturbation to the magnetic properties. Moreover, the incommensurate structure induces mutual lattice modulation in the RS and TaS_2 sublattices, so that magnetic interactions or magnetic anisotropy are strongly modified through the modified crystal-field effect. It is known that $(RS)_xTaS_2$ has quite low magnetic transition temperatures in comparison with pristine RS. The magnetic interaction in the stacking direction is weakened by separation in space, and the Ruderman-Kittel-Kasuya-Yosida (RKKY) interaction, which is the dominant magnetic interaction in pristine RS, is strongly reduced.[4]

Among compounds analogous to $(RS)_xTaS_2$, it is known that sulfides with divalent metals, e.g., Sn^{2+} in SnS, are inserted into the galleries of TaS_2 layers,[1] as well as those with trivalent metals. When RS has stable states of both R^{2+} and R^{3+}, $(RS)_xTaS_2$ can give a mixed valence state of R. Pristine samarium monosulfide SmS is semiconducting, with an ionic state of $Sm^{2+}S^{2-}$, and exhibits a valence change of Sm from divalent to intermediate states under high pressure above 6.5 kbar.[5] The valence state of Sm in SmS under high pressure is not a well-localized trivalent but a mixing state of 4*f* and conduction electrons, i.e., the valence fluctuation. Therefore it is interesting to investigate which valence state among Sm^{2+}, Sm^{3+}, or Sm^{2+}/Sm^{3+} mixing states is realized in $(SmS)_{1.19}TaS_2$ when SmS double layer is introduced between the TaS_2 slabs. Physical properties of this compound[4,6] and the NbS_2 analog[7] have been reported; how-

0163-1829/93/48(15)/11077(9)/$06.00

ever, the interpretation of the valence state of Sm is still controversial.

In this paper we report the resistivity, thermoelectric power, magnetoresistance, Hall coefficient, magnetic susceptibility, and x-ray photoemission spectroscopy (XPS) measurements of $(SmS)_{1.19}TaS_2$ and clarify the valence state of Sm. We also discuss the effect of the lattice incommensurability on the electronic structure of $(SmS)_{1.19}TaS_2$.

II. EXPERIMENTS

Single crystals of $(SmS)_{1.19}TaS_2$ were prepared by the chemical vapor transport method using iodine. A mixture of the constituent element powers in portions according to their chemical composition was sealed in an evacuated quartz tube under 10^{-5} torr, and heat treated in a two-zone furnace with the temperature gradient 950–850 °C for one or two weeks. The single crystals obtained were very thin platelets with a typical dimension of 3×3 mm^2 with 5–10-μm thickness. Most of the crystals contain stacking faults, as microscopically observed by electron diffraction, since the RS layer can grow along six equivalent directions on the TaS_2 layer. The crystals were characterized by x-ray and electron diffraction and were ascertained isostructurally to that determined by single-crystal x-ray analysis.[6] Resistivity measurements were carried out by usual four-probe method using gold wires and silver paints. The magnetoresistance and Hall coefficient were measured up to 7 T in the temperature range of 1.3–30 K, with magnetic field applied parallel to the c axis. The thermoelectric power was measured by detecting the temperature gradient by using Au(Fe)-Chromel thermocouples from 4.2 to 300 K. The magnetic susceptibility was measured by a Faraday balance under 2 T from 1.9 to 280 K, and the magnetization was measured up to 5.2 T at 1.9 and 4.3 K with magnetic fields perpendicular and parallel to the crystallographic c axis. The x-ray photoemission spectra were measured by VG-scientific MK-2 using a source radiation of Al (1486.6 eV) and Mg (1253.6 eV) under vacuum higher than 10^{-9} torr. The sample surface was etched by an ionized argon beam to about 10 Å in depth in order to remove surface oxidization, and heat treatments were successively made at 200 or 250 °C to repair the damaged surface.

A. Results

The in-plane resistivity ρ of $(SmS)_{1.19}TaS_2$ is shown in Fig. 1 as a function of temperature. The resistivity shows a linear temperature dependence with a large residual resistivity of 120 $\mu\Omega$ cm, which corresponds to a small residual resistivity ratio R(r.t.)/R(4.2 K) of 2.2. These features are almost identical to those for the isostructural compounds $(RS)_xTaS_2$ with other R metals. The linear temperature dependence of ρ suggests that the temperature-dependent scattering is due only to the acoustic phonon. The residual resistivity comes from temperature-independent carrier scattering associated

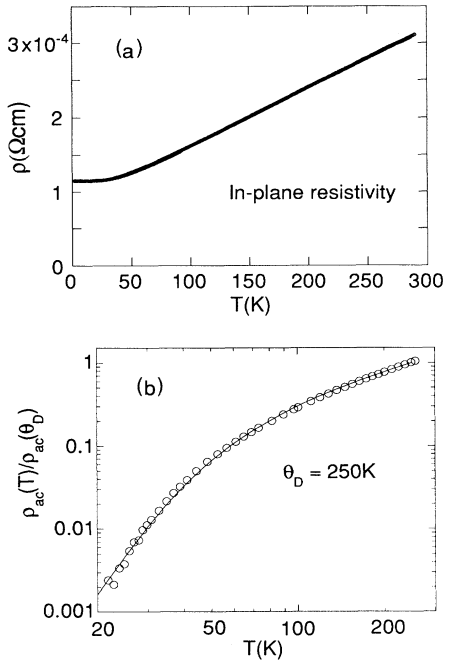

FIG. 1. (a) The temperature dependence of the resistivity ρ of $(SmS)_{1.19}TaS_2$. The behavior is similar to those of other $(RS)_xTaS_2$. (b) Logarithmic plot of the temperature dependence of the phonon resistivity normalized at the fitted Debye temperature. The fitting curve according to Eq. (1) is shown by the solid line.

with impurities or lattice imperfection including incommensurate potential characteristics in $(RS)_xTaS_2$. Grüneisen's equation[8] for the acoustic-phonon part $[\rho_{ac}=\rho(T)-\rho(0)]$ is expressed with Debye temperature θ_D as

$$\frac{\rho_{ac}(T)}{\rho_{ac}(\theta_D)}=\left[\frac{T}{\theta_D}\right]^5\int_0^{\theta_D/T}\frac{x^5}{(1-e^{-x})(e^x-1)}dx\ . \qquad (1)$$

By fitting the resistivity to Eq. (1), we evaluate $\theta_D=250$ K. This value is close to θ_D of the isostructural compound $(LaS)_{1.13}NbS_2$.[9]

Figure 2 shows the temperature dependence of the thermoelectric power S of $(SmS)_{1.19}TaS_2$. S is positive in the measured temperature range, suggesting the predominant hole carriers. As temperature is increased, S increases with a convex curvature up to 120 K and shows linear temperature dependence above 120 K. The deviation from the linear temperature dependence at low temperatures is ascribed to the phonon drag effect, and at high temperatures the electron diffusion is predominant. We will discuss the thermoelectric power in Sec. II B.

The temperature dependence of the resistivity and thermoelectric power of $(SmS)_{1.19}TaS_2$ is almost identical to that of other isostructural $(RS)_xTaS_2$ (Refs. 3 and 4) with R^{3+}. In this respect the electronic structure of $(SmS)_{1.19}TaS_2$ is not different from that of other trivalent R compounds. In contrast, the thermoelectric power of the isostructural $(PbS)_{1.13}TaS_2$ (Ref. 10) and $(SnS)_{1.17}NbS_2$

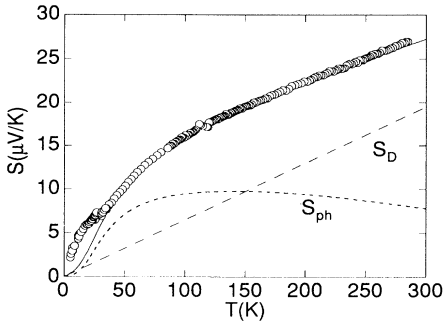

FIG. 2. The temperature dependence of the thermoelectric power of $(SmS)_{1.19}TaS_2$ is denoted by circles. The solid line represents the fitting curve of the total thermoelectric power. S_D and S_{ph} are the calculated contributions of the electron diffusion (dashed line) and phonon drag (dotted line) terms, respectively.

(Ref. 11) shows quite a different behavior, the value of which is negative at room temperature. Pb and Sn atoms are considered to be divalent in both pristine PbS and SnS and their inserted compounds.

Hall voltages of $(SmS)_{1.19}TaS_2$ increase linearly with increasing magnetic field up to 7 T. The Hall coefficients R_H are nearly independent of temperature between 1.5 and 30 K, where the variation of R_H is within 2%. The carrier concentration n estimated from the single carrier model $R_H=-1/ne$ is 0.052 holes per formula unit of $(SmS)_{1.19}TaS_2$. This value agrees with the value of 0.04 previously reported.[6]

Figure 3 shows the magnetoresistance $\Delta\rho(H)/\rho(0)$ $[\Delta\rho(H)=-\rho(H)-\rho(0)]$ of $(SmS)_{1.19}TaS_2$ at 4.2 K as a function of magnetic field H up to 7 T. $\Delta\rho(H)/\rho(0)$ shows a quadratic field dependence whose magnitude reaches only 0.004 at 7 T. The magnetoresistance originates from the presence of carriers with different masses, so that $(SmS)_{1.19}TaS_2$ has a multicarrier system, or a single carrier system with a closed Fermi surface deformed from a circular one to some extent. The experimental facts of extremely small magnetoresistance and its weak temperature dependence in $(SmS)_{1.19}TaS_2$ suggest that the compound has a single hole carrier electronic system.

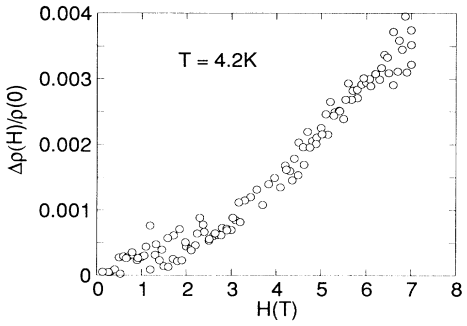

FIG. 3. The magnetic-field dependence of the in-plane magnetoresistance $\Delta\rho(H)/\rho(0)$. Magnetic fields are applied along the c axis (normal to the plane).

The temperature dependence of the magnetic susceptibility of $(SmS)_{1.19}TaS_2$ is shown in Fig. 4 under magnetic fields parallel ($H_\parallel c$) and perpendicular ($H_\perp c$) to the crystallographic c axis. The calculated susceptibility for free Sm^{2+} and Sm^{3+} ions, taking into account spin-orbit interaction,[12] is also shown for comparison. The susceptibility of free Sm^{2+} reaches a constant value, with temperature going to zero because of the ground state $J=0$. For free Sm^{3+} ($J=\frac{5}{2}$), the susceptibility obeys the Curie law including the contribution of the higher J state at higher temperatures. The observed susceptibility of $\chi_\parallel(H_\parallel c)$ at room temperature lies between the calculated values for free Sm^{2+} and Sm^{3+} ions. The temperature dependence of the inverse susceptibility $1/\chi_\parallel$ above 60 K [see Fig. 4(b)] is almost linear with a slightly downward curvature. By fitting the Curie-Weiss law, we estimate the Weiss temperature $\theta_\parallel=-55$ K and the Curie constant $C_\parallel=0.66$ emu K/mol, the latter corresponding to the effective magnetic moment $\mu_{\rm eff}=2.28\mu_B$/Sm. Below 60 K, $\chi_\parallel$ deviates from the Curie-Weiss curve toward lower values and exhibits a small hump at 30 K, and finally steeply increases as temperature is lowered. The susceptibility $\chi_\perp(H_\perp c)$ exhibits different behavior from $\chi_\parallel$. The susceptibility $\chi_\perp$ at room temperature is close to the value for free Sm^{3+}. Above 60 K, $\chi_\perp$ roughly obeys the Curie-Weiss law where $\theta_\perp$ and $C_\perp$ are estimated at -80 K and 0.332 emu K/mol, respectively. The latter corresponds to $\mu_{\rm eff}=1.63\mu_B$/Sm, which is 30% smaller than

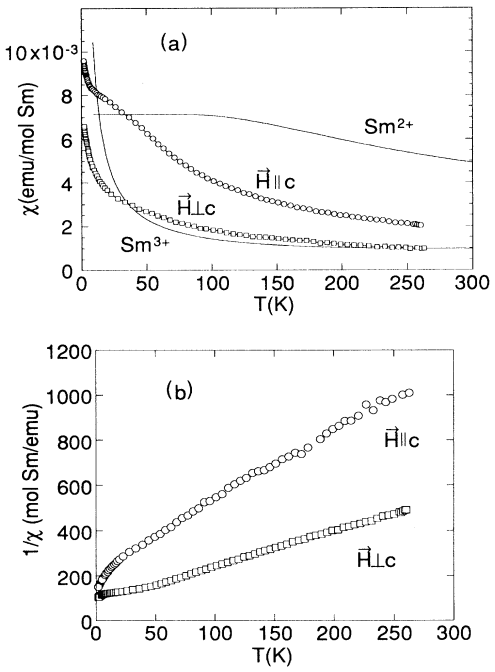

FIG. 4. (a) The temperature dependence of the magnetic susceptibility of $(SmS)_{1.19}TaS_2$ for $H_\parallel c$ and $H_\perp c$. Solid lines indicate the calculated susceptibility for free Sm^{3+} and Sm^{2+}. (b) Reciprocal resistivity of $(SmS)_{1.19}TaS_2$ for $H_\parallel c$ and $H_\perp c$.

that estimated from $\chi_{\parallel}$. Below 60 K, contrary to the behavior of $\chi_{\parallel}$, $\chi_{\perp}$ increases more rapidly than the fitted Curie-Weiss curve with decreasing temperature.

Free Sm^{3+} ions have an effective moment of $0.86\mu_B$. In general, the magnetic susceptibility of Sm compounds does not obey the simple Curie-Weiss law due to the spin-orbit interaction, which changes its temperature dependence as if the effective moment is increased. The difference between the observed and the expected moments is due to this effect. The fact that the susceptibility depends on the direction of applied magnetic fields indicates that the crystal field works significantly on magnetic Sm ions, and hence, Sm^{3+} is dominant in $(SmS)_{1.19}TaS_2$ since the crystal field works only on Sm^{3+}.

The 3*d* core-level x-ray photoemission spectra using a radiation source of Al are shown in Fig. 5. The spectra consist of two sets of peaks assigned to Sm^{3+} with binding energies (B.E.) of 1083 ($3d^{5/2}$) and 1110 eV ($3d^{3/2}$), and Sm^{2+} with B.E. of 1073 ($3d^{5/2}$) and 1100 ($3d^{3/2}$), respectively. The data were taken at first without argon etching, where the spectra show a remarkable oxygen 1*s* photoemission (B.E.=581 eV) peak. In the Sm 3*d* region, peaks of the Sm^{2+} state are considerably weak, as seen in Fig. 3(a), since the sample surface is oxidized to form Sm_2O_3 and a portion of the Sm^{2+} peak is reduced. Similar results have been obtained for $(CeS)_{1.14}TaS_2$, where CeO_2 is formed and the spectra exhibit peaks from the Ce^{4+} ($4f^0$) initial state.[13] Therefore ionized argon etching was made until the O 1*s* peak disappeared, and then the spectra were taken immediately before the surface was oxidized again. After the sample treatment, the Sm^{2+} peaks were increased to the Sm^{2+}/Sm^{3+} ratio of $\frac{1}{4}$. However, as the sample surface was rather damaged by Ar^+ beams, we performed a heat treatment at 200 or 250 °C, carefully monitoring the O 1*s* peak. After the annealing the intensity of the Sm^{2+} peak decreased by removing the surface state. From the final spectra [Fig. 5(c)], the portion of Sm^{2+} in $(SmS)_{1.19}TaS_2$ is estimated to be 0.12. The same result was obtained by using another source radiation of Mg (1253.6 eV), although the Auger peak of sulfur ($K_{\alpha\beta}$) was superimposed onto the photoemission peak from the Sm^{2+} $3d_{3/2}$ initial state.

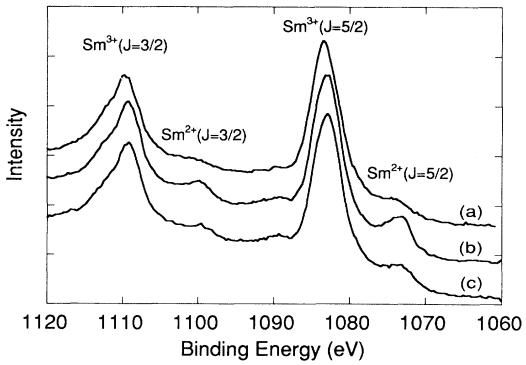

FIG. 5. Core-level X-ray photoemission spectra for $(SmS)_{1.19}TaS_2$ (Sm 3*d* region). (a) As-grown sample. (b) After argon etching. (c) After annealing at 250 °C. Note that the relative intensities of the peaks from the Sm^{2+} initial state changes markedly from (a) to (c).

B. Discussion

1. *Analysis of the thermoelectric power of* $(SmS)_{1.19}TaS_2$

First we consider the electronic structure of $(SmS)_{1.19}TaS_2$ from transport properties. The temperature and magnetic-field dependence of the magnetoresistance and Hall coefficient show that the dominant carriers in $(SmS)_{1.19}TaS_2$ are holes with a small carrier density (0.052 holes per TaS_2). The presence of hole carriers is well explained by the incomplete electron transfer from SmS to TaS_2 on the basis of a rigid band description. According to the band calculation for $2H$-TaS_2,[14] the conduction band is mainly formed of the half-filled TaS_2 $5d_z^2$ orbital, with two kinds of Fermi surfaces and marked energy dispersion along c^* direction due to the interlayer interaction. In $(SmS)_{1.19}TaS_2$, the small concentration of hole carriers and the single carrier electrical conduction mentioned in Sec. II A suggests that the electron transfer from SmS to TaS_2 makes the TaS_2 conduction band nearly full and the size of the cross-sectional area of the Fermi surfaces diminishes. In addition, because of the presence of SmS between TaS_2 layers, the conduction band of TaS_2 loses the energy dispersion along the c^* direction and forms a cylindrical Fermi surface. More detailed discussions of the band structure will be made below, but here we assume a free-electron model with a cylindrical Fermi surface for $(SmS)_{1.19}TaS_2$ in order to fit the temperature dependence of thermoelectric power S.

Thermoelectric power can be expressed by the sum of the electron diffusion term S_D and the phonon drag term $S_{\rm ph}$:

$$S = S_D + S_{\rm ph} \ . \tag{2}$$

Using the Mott formula, the electron diffusion term is derived as[15]

$$S_D = \frac{\pi^2 k_B^2}{3e} \left[\frac{\partial \ln\sigma}{\partial E} \right]_{E_F} , \tag{3}$$

where k_B is the Boltzmann constant, e is the charge of an electron, σ is the electrical conductivity, and E_F is the Fermi energy. Since the electron-phonon-scattering time τ involved in σ is independent of energy in the two-dimensional free-electron system with a parabolic energy dispersion,[15] the diffusion term is expressed as

$$S_D = \frac{\pi^2 k_B^2}{3e} \frac{T}{E_F} \ . \tag{4}$$

The phonon drag term is given by

$$S_{\rm ph} = \frac{\langle C_p R \rangle}{3en} , \tag{5}$$

where C_p is the specific heat of acoustic phonons which contribute to the phonon drag effect, and n is the carrier density. $R(q)$ represents the momentum transfer ratio of the electron phonon scattering to all contributions from

phonon-scattering processes. The momentum transfer of phonon in a unit time depends on the kind of scattering, which is proportional to q by electron-phonon scattering, independent of q or T by domain boundary scattering, and proportional to q and T^3 by phonon-phonon scattering:

$$R(q)=\frac{aq}{b+aq+cqT^3} , \tag{6}$$

where b is the number of collisions by domain boundaries in a unit time, and a and c are coefficients of the electron-phonon and phonon-phonon interaction, respectively. From Eq. (5), the phonon drag term is given by the following equations:

$$S_{\rm ph}=\frac{k_B^2T^2}{4e\hbar^2k_F^2v_s^2}\int_0^{x_{\max}}\frac{x^3e^x}{(e^x-1)^2}R(x)dx , \tag{7}$$

$$x=\frac{\hbar v_s q}{k_BT} , \tag{8}$$

$$x_{\max}=\frac{\hbar v_s q_{\max}}{k_BT} , \tag{9}$$

where k_F is the Fermi wave number, v_s is the sound velocity of the acoustic phonon, and $q_{\max}$ is the maximum phonon frequency available for the momentum transfer through the phonon drag process, namely $q_{\max}=2k_F$.

In the low-temperature region, the thermoelectric power of $(SmS)_{1.19}TaS_2$ has a small hump around 30 K. This anomaly comes from the experimental inaccuracy, which includes the thermoelectric power of gold wires used in this measurement. Therefore, we omit the low-temperature data for the theoretical fit. The linear temperature dependence of S at higher temperatures indicates that the electron diffusion term S_D is predominant in the temperature region. Using the above equations (2)–(9), we obtain a good agreement between the experimental and calculated thermoelectric power with the following fitting parameters:

$$b/aq_{\max}=1.7\pm0.2 ,$$

$$c/a=3\pm2\times10^{-8}\ \mathrm{K}^{-3} ,$$

$$k_Fv_s=1.1\pm0.05\times10^{13}\ \mathrm{s}^{-1} ,$$

$$E_F=0.44\pm0.04\ \mathrm{eV} .$$

The calculated thermoelectric power S_D and $S_{\rm ph}$ is drawn in Fig. 2. The low Fermi energy $E_F=0.44$ eV stands for the small concentration of the conduction carriers, which fact supports the assumption that the conduction band of TaS_2 is almost filled by the electron transfer from SmS. This value agrees fairly well with the Fermi energy $E_F=0.54$ eV obtained from reflectivity measurements.[16] In comparison with the dispersion curves and density of states of the conduction band calculated by Mattheiss,[17] the obtained Fermi energy $E_F=0.44$ eV corresponds to a carrier density of less than 0.1 holes per TaS_2, consistent with the carrier density of 0.052 obtained from the Hall coefficient measurements. The Fermi wave number k_F is estimated at $4.2\times10^9\ \mathrm{m}^{-1}$ using the relation $E_F=\hbar k_F^2/m^*$, where the band mass $m^*=1.4m_e$ is known for TaS_2. Using the fitted value of k_Fv_s, the sound velocity for the acoustic phonon is estimated at 2.6×10^3 m/s. The velocity is related to the Debye temperature θ_D as

$$\theta_D=\frac{\hbar v_s}{k_BT}(6\pi^2N) , \tag{10}$$

where N is the atomic density. From Eq. (10) and the estimated sound velocity, the Debye temperature is calculated to be 290 K. This value agrees with the result obtained from the electrical resistivity mentioned in Sec. II A. By comparison of values a, b, and c, we know the character of phonon scattering in $(SmS)_{1.19}TaS_2$. The fitted values a, b, and c suggest that contributions from these three types of phonon scattering are comparable at around room temperature. The ratio of the domain boundary scattering to the electron-phonon scattering b/aq is 1.7 at $q=q_{\max}$. If we assume that the domain boundary scattering is negligible ($b=0$) while other parameters are held at their fitted values, the phonon drag contribution is unrealistically enhanced by about three times the fitted one. Therefore the phonon scattering at domain boundaries significantly reduces the phonon drag effect. This fact is consistent with the presence of the large residual resistivity associated with the carrier scattering by domain boundaries. The phonon-phonon-scattering term is not so effective for the thermoelectric power, because the electron diffusion term is dominant at high temperatures, as known from the linear temperature dependence of the thermoelectric power.

To summarize this section, we elucidate the process of phonon scattering by analysis of the thermoelectric power of $(SmS)_{1.19}TaS_2$. The contribution of domain boundary scattering to the total phonon scattering is significant in this compound. It is considered that the domain boundary scattering is brought about by the lattice incommensurability, which induces domain boundaries by forming a discommensuration structure. Although quite a simple model is used in the above treatment, the obtained picture of the electronic and lattice structures accounts for the values of the Fermi energy and the Debye temperature and the presence of boundary scattering attained by experiments. Therefore, the single carrier description on the basis of the TaS_2 conduction band is effective for $(SmS)_{1.19}TaS_2$.

2. *Magnetism and valence state of $(SmS)_{1.19}TaS_2$*

Next we consider the valence state of Sm from the magnetic susceptibility. As one can see in Fig. 4, the susceptibility of $(SmS)_{1.19}TaS_2$ is not expressed simply by the contribution of Sm^{2+}, whose susceptibility becomes a constant value at low temperatures. The strong anisotropy in the susceptibility indicates the presence of the crystal-field effect. The crystal field works on the spin state of Sm^{3+} ($J=\frac{5}{2}$), specifically because $J=0$ in Sm^{2+}. It is known that the lattice constants of $(SmS)_{1.19}TaS_2$ are those expected for Sm^{3+}, whose values are affected by the lanthanide contraction for the series of $(RS)_xTaS_2$ with

trivalent R.[3] These facts suggest the strong contribution from the Sm^{3+} state to the susceptibility. If we assume that $(SmS)_{1.19}TaS_2$ consists only of Sm^{3+}, it is necessary to consider a large antiferromagnetic interaction ranging larger than 50 K, as expected from the temperature dependence of the inverse susceptibility ($\theta_{\parallel}=-55$ K and $\theta_{\perp}=-80$ K). The inclusion of such large interaction is, however, inconsistent with the absence of the magnetic ordering down to 2 K. The Weiss temperatures of other $(RS)_xTaS_2$ are known to be lower than 10 K. Some of them show antiferromagnetic transition at low temperatures, whose transition temperatures T_N are 2.0, 4.1, and 1.7 K for Ce, Gd, and Dy compounds, respectively, and Nd and Er compounds are known to have no magnetic transition down to 1.2 K.[2] Since the electrical transport and structural properties are quite similar to each other in the $(RS)_xTaS_2$ family, the similar magnitude of exchange interaction is expected in $(SmS)_{1.19}TaS_2$. Therefore, the large antiferromagnetic interaction should be excluded.

According to the crystal structure study of $(SmS)_{1.19}TaS_2$, the Sm ions are coordinated by five sulfur atoms in the SmS layers and two or three sulfur atoms in the adjacent TaS_2 layers,[6] and their bond lengths are not the same. Such an asymmetric environment of coordination of sulfur comes from the peculiar crystal structure of $(SmS)_{1.19}TaS_2$, where the SmS layers consist of a sliced NaCl-type double-layer structure having layers incommensurate with TaS_2. Therefore the electric crystal field associated with the coordinated sulfurs varies depending on the location of Sm sites. The sixfold-degenerate Sm^{3+} $4f$ level ($^6H_{5/2}$) is split into three doublets by the crystal field,[17] and the energy arrangement of these three levels is different in each Sm site. Such a situation makes accurate calculation of the total susceptibility difficult, even though, as in the case of the susceptibility of $(SmS)_{1.19}TaS_2$, the unrealistically large Weiss temperature θ, the anisotropic magnetic moments μ_{eff}, and the deviation of the susceptibility from the Curie-Weiss law in the low-temperature region, are not ascribed to the crystal field effect entirely. Therefore it is necessary to include the contribution of the divalent state of Sm to account for the behavior of the susceptibility in the whole temperature range.

The XPS spectra give clear evidence that $(SmS)_{1.19}TaS_2$ has the mixed valence state of Sm^{2+} and Sm^{3+}. As to the origin of the XPS peaks, we have to consider the shakedown process. During the photoemission process in rare-earth compounds with a number n of $4f$ electrons, the lowest $4f$ final state has one more $4f$ electron supplied from the conduction band since the state is stabilized through the Coulomb interaction between the $4f$ electrons and the core holes created by photoemission. The satellite peaks arising from the final state are often found in light rare-earth intermetallic compounds. The intensity of the peak from the final state essentially relies on the strength of the hybridization between the conduction bands and the $4f$ state. The hybridization decreases as rare earths become heavier, since the $4f$ state becomes lower from the Fermi energy. Thus the final-state satellites in Sm compounds are too weak to be observed, as known from the series of RPd_3 alloys.[18] It is considered that the hybridization effect is more weakened in $(SmS)_{1.19}TaS_2$ than in metallic Sm compounds, since the conduction carrier is not present in the SmS part, as discussed below. Therefore the observed peaks at the Sm^{2+} positions are yielded purely by the Sm^{2+} initial state. Another possibility for the appearance of the Sm^{2+} peak is one originating from the surface state. The kinetic energy of the photoelectron in the Sm $3d$ region is about 300 eV when we employ the source radiation of Al. The escape depth l of the photoelectron from the inside of the sample is related to its kinetic energy,[19] and the kinetic energy of 300 eV corresponds to l of 8 Å. Since the thickness of the TaS_2 layer is about 6 Å, the Sm $3d$ electrons can escape not only from the surface SmS layer but also from the second SmS layer whose surface is covered by a TaS_2 layer. Therefore, it is considered that the observed XPS spectra give the bulk properties of $(SmS)_{1.19}TaS_2$. Taking account of these points, we conclude that the valence mixing of Sm^{2+} and Sm^{3+} is realized in $(SmS)_{1.19}TaS_2$. By using the $Sm^{2+}/Sm^{3+}=0.12$ obtained from the XPS data, the room-temperature susceptibility is calculated to be 1.3×10^{-5} emu/g. This value is very close to the geometric mean value $\chi_m=\sqrt[3]{\chi_{\parallel}\chi_{\perp}^2}$ of 1.27×10^{-5} emu/g.

3. *Conduction mechanism in $(RS)_xTaS_2$*

Next we discuss the conduction mechanism in $(SmS)_{1.19}TaS_2$. The conduction mechanism is assumed to be common in the isostructural series $(RS)_xTaS_2$ because of the similarity in the transport properties. Therefore, at first, we discuss the conduction mechanism of $(RS)_xTaS_2$ generally. As applied in the transition-metal dichalcogenide intercalation compounds, we employ a simple rigid band model for the electronic structure of $(RS)_xTaS_2$ where electrons on the RS conduction band are transferred to the TaS_2 conduction band. The conduction band of the pristine TaS_2 consists mainly of the Ta $5d_Z^2$ orbital, which is lowest lying in the Ta $5d$ levels split by the trigonal crystal field. Conduction electrons occupy half of this band, resulting in the metallic state of TaS_2.[14] In pristine RSs with NaCl crystal structure, the conduction band is formed of the R $5d$ and $6s$ orbitals. The electronic structure of RS depends on the valence state of R, namely it is metallic for R^{3+} and semiconductor for R^{2+}. The latter case is known for SmS and EuS in the series of RS. In the incommensurate layer compounds $(RS)_xTaS_2$, inserted RS layers are sliced parallel to the {100} plane of the pristine structure and form a double layer between the TaS_2 layers. Then the electronic structure of the inserted RS layers is modified from pristine RS. Interest consists in the nature of the transferred electrons to TaS_2; that is, which electrons in the $4f$ state or the conduction band of RES are transferred to TaS_2.

According to the results of the Hall effect, magnetoresistance, and thermoelectric power measurements, it is considered that the electrical conduction in this system

is described in terms of one kind of hole carrier in the TaS_2 conduction band. In addition, physical properties of $(RS)_xTaS_2$ are known to have the following features:[3,4] (i) the temperature dependence of ρ and the residual resistivity ratio RRR are almost identical for all compounds of $(RS)_xTaS_2$; (ii) no anomaly is observed in the temperature dependence of ρ at magnetic transition temperatures (T_N) in antiferromagnetic R=Ce, Gd, and Dy compounds; (iii) T_N is considerably reduced from T_N of pristine RS in the above compounds; and (iv) the semiconducting vanadium analogues $(RS)_xVS_2$ (Ref. 20) have higher T_N than $(RS)_xTaS_2$. The absence of R dependence in the transport properties suggests that the electrical conduction is governed by the carriers on the TaS_2 conduction band. The absence of the magnetic ordering effect in the transport properties and the reduction of magnetic transition temperatures implies that the spin polarization of the conduction electron does not develop around the magnetic R atoms, namely, the carriers do not exist in the RS layers. All these experimental facts prove that the carriers exist only in the TaS_2 layers.

Taking into consideration the nonstoichiometric composition of $(RS)_xTaS_2$ ($x=1.13-1.23$),[3] the electron transfer from RS is not completed for the following reason. It is known in TaS_2 intercalation compounds that at most one electron per TaS_2 is transferred from the intercalate species, because the TaS_2 conduction band is half filled, and to transfer more than one electron requires energy beyond the d-d energy gap of the TaS_2 $5d$ band.[21] Even if the maximum electron transfer occurs, that is, one electron per TaS_2 corresponding to $1/x$ electrons per RS unit is transferred, $(1-1/x)$ electrons still remain in the RS conduction band because $x>1$. The value of $(1-1/x)$ increases from 0.13 to 0.2 by increasing the atomic number of R from La to Er. Judging from the experimental results, the existence of hole carriers in the TaS_2 conduction band evidently suggests that the electron transfer is less than one per TaS_2. This implies that a significant number of carriers should remain in the RS layer, predicting a metallic state for the RS layer. The carriers, however, do not take part in the electrical conduction in $(RS)_xTaS_2$.

The band structure of pristine RS predicts that the carriers remaining on the RS layer are electronlike[22] and have a larger density than the hole carriers observed in the TaS_2 layer. If the electron carriers are mobile, their mobility should be smaller than that of the observed holes because R_H is independent of temperature and magnetic field. If the mobile carriers exist in the RS layers, they can mediate the RKKY interaction between magnetic R ions. Then some anomalies will appear in the resistivity at the magnetic transition temperature, and the magnetic transition temperature is not reduced significantly from that of the corresponding pristine RS. The presence of the RKKY interaction as a dominant magnetic interaction contradicts the experimental facts. For example, semiconducting $(CeS)_{1.19}VS_2$ has higher T_N (5.5 K) (Ref. 20) than metallic $(CeS)_{1.14}TaS_2$ (2.0 K),[3] and T_N of $(GdS)_{1.20}TaS_2$ is reduced to 4.1 K from 40 K of the pristine GdS whose exchange interaction is dominated by the RKKY interaction. Therefore it is considered that the observed hole carriers are separated in space from R ions, and the remaining electrons on the RS conduction band are localized.

There is a question as to why the carriers in the RS layers do not take part in the electrical conduction. To answer this, we discuss the effect of lattice incommensurability on the electrical conduction of $(RS)_xTaS_2$. The most marked characteristic in this system is the lattice misfit between RS and TaS_2 sublattices. Their lattice constants are fitted to each other in the b direction, while they are almost independent in the a direction with an irrational (incommensurate) ratio. Consequently the lattice incommensurability induces mutual lattice modulation to the TaS_2 and RS sublattices. Evidence of the strong incommensurate modulation of the sublattices is found in the electron diffraction of $(RS)_xTaS_2$, which contains satellite spots along the incommensurate direction.[23] The satellite spots have comparative intensity with the main spots, so that the mutual modulation is notably strong.

The lattice incommensurability yields disordered and quasiperiodic potentials that scatter the carriers. The quasiperiodic potential acts one dimensionally and generates energy gaps in the conduction bands. In this respect, $(RS)_xTaS_2$ is a good example of the problem of an electronic system with one-dimensional quasiperiodic potentials. Tight-binding calculations[24-27] for a linear chain with a quasiperiodic potential recently showed the possibility of carrier localization. If a quasiperiodic potential with the period a' is added to a system with the period a, the potential is possible to open energy gaps at $\pm\pi/na'$ with optional integers n in the one-dimensional band. In the calculations, the quasiperiodicity $\omega=a/a'$ is at first approximated to be the simplest rational number n/m. The energy gap appears at the position corresponding to the lattice period ma. It is also found that the intragap states appear as the approximation proceeds by taking more complicated rational numbers.

In $(RS)_x$ TaS_2, the quasiperiodic potential is related to the lattice constants in the incommensurate direction, a_{TaS_2} and a_{RS}. The conduction band of RS is affected by the quasiperiodic potential from TaS_2. This potential makes energy gaps at the wave numbers $q_n=\pm\pi/na_{TaS_2}$ with optional integers n in the first Brillouin zone. The wave numbers q_n are common in $(RS)_xTaS_2$, since a_{TaS_2} is nearly the same (~ 3.31 Å) in the compounds. If there are any integers m that nearly satisfy the relation $na_{TaS_2}=ma_{RS}$, the effect of the quasiperiodic potential is made stronger through the formation of m-fold superstructures in the RS sublattice. The ratio a_{RS}/a_{TaS_2} ranges between 1.77 and 1.623 (Ref. 3) by varying the R element so that the value m depends on $(RS)_x$ TaS_2. In $(SmS)_{1.19}TaS_2$, the ratio $a_{SmS}/a_{TaS_2}=1.689$, therefore $n/m=17/10$ is taken as a rational number close to a_{SmS}/a_{TaS_2}, for instance. Accordingly, a tenfold superlattice is preferentially formed along the incommensurate direction in the SmS sublattice. In the two-dimensional electronic system, the quasiperiodic potential generates a

zone-folding effect in the conduction band instead of the one-dimensional energy gap. In this case, after the carriers stop moving in the incommensurate direction due to the quasiperiodic potential, the carriers can move within the other direction.

The lattice incommensurability also induces the random potential in actual compounds through the formation of the discommensurate structure mentioned above. If the random potential is formed as a result of relaxation of the local stress of individual atoms, the carriers experience additional scattering from the random potential. This causes localized electronic states with a mobility edge in the conduction band. The charge transfer reduces the numbers of the conduction carriers and the Fermi energies in both the TaS_2 and RS conduction bands from those in the pristine compounds. The lowering of the Fermi energy, namely, the reduction of the kinetic energy of conduction carriers, favors the carrier localization. Thus the localized feature of the conduction carriers in the RS part is associated with the random potential and/or the one-dimensional instability.

The metallic behavior of $(RS)_xTaS_2$ means that the carriers in the TaS_2 part are not localized. The S-Ta-S sandwich structure of the TaS_2 layer is sustained in $(RS)_xTaS_2$, and the structure is less modulated from the pristine one than in the RS layer.[3] Therefore, it is supposed that the quasiperiodic potential associated with the lattice incommensurability does not give significant modification of the band structure of TaS_2. In contrast to $(RS)_xTaS_2$, the semiconductive conduction in $(RS)_xVS_2$ suggests that the carrier localization in the VS_2 part is realized as well as in RS in $(RS)_xVS_2$.[20]

In the pristine compound SmS, the Sm $4f^6$ energy level is lower than the bottom of the Sm $5d$-$6s$ conduction band, so that the SmS is a semiconductor. The application of pressure broadens the conduction band and mixes it with the Sm $4f^6$ level, which leads the SmS to be metallic with a Sm valence fluctuation state.[4] For a double layer of SmS in $(SmS)_{1.19}TaS_2$, it is not known whether the Sm $4f^6$ level or the Sm $5d$-$6s$ conduction band is lower. If the double layer of SmS has an electronic structure resembling the pristine one, conduction electrons can remain in the Sm $4f^6$ level.

According to Hall effect measurements, which suggests that the compound has hole carriers ($0.052/TaS_2$) only in the TaS_2 conduction band, the concentration of electrons transferred to TaS_2 is 0.948 per TaS_2. Consequently, $0.20(=1-0.948/1.19)$ electrons remain in the SmS layer. In $(SmS)_{1.19}TaS_2$, the ratio between the lattice constants of SmS and TaS_2 sublattices is 1.689 along the incommensurate direction. Close to this value, 17/10 is considered as a simple rational number, so that the superlattice with the period of $10a$ (a is the lattice constant of the SmS sublattice) will be realized. Hence the energy gap appears at the wave number $k=\pm\pi/10a$ in the a^* direction, where the lowest band can accommodate 0.2 electrons per $(SmS)_{1.19}TaS_2$. In fact, $(SmS)_{1.19}TaS_2$ has a two-dimensional electronic structure, so that the one-dimensional potential gives a zone-folding effect to the energy band in the a^* direction, whose lowest band can accommodate 0.2 electrons. The electrons can move with a wave vector along the b^* direction. We consider that the carriers are affected by some random potentials in this direction to make whole carriers localized.

The electronic state of $(SmS)_{1.19}TaS_2$ is not simple, because, from the XPS measurement, there are 0.12 electrons in Sm^{2+} $4f^6$ level. This means that the Fermi level is located in the Sm $4f^6$ level. The difference between these two values 0.2 and 0.12 suggests that the Sm $4f$ state mixes with the SmS conduction band, i.e., the valence fluctuation, and all the electrons in the SmS layers are localized by the quasiperiodic and random potentials.

III. CONCLUSION

We measured the resistivity, thermoelectric power, magnetoresistance, Hall effect, magnetic susceptibility, and x-ray photoemission spectra of $(SmS)_{1.19}TaS_2$ in order to investigate the valence state of Sm and the effect of the lattice incommensurability. The transport properties indicate that the electrical conduction is dominated by only one kind of hole carrier which is isolated on the TaS_2 layer, and the carriers on the RS layer are silent in the electrical conduction. This fact is intensively supported by the experimental result that the magnetoresistance and Hall coefficient are independent of magnetic field and temperature. The temperature dependence of the thermoelectric power is analyzed in terms of the electron diffusion and phonon drag contributions. The fitted values of the Fermi energy and the Debye temperature are coincident with those obtained by optical[16] and resistivity measurements. The susceptibility and XPS measurements reveal that the system has a valence mixing state of Sm^{2+} and Sm^{3+}, where the portion of the Sm^{2+} is estimated at 0.12. We also discussed the conduction mechanism of the series of $(RS)_xTaS_2$ consisting of a nonconducting RS part and a metallic TaS_2 part, and proposed that the carriers on the RS part are localized due to the quasiperiodic potential created by the lattice incommensurability. In the Sm compound, the valence fluctuating SmS conduction electrons are considered to be localized by this potential.

Recently, we found that the analogous compounds $(RS)_xVS_2$ ($x=1.15\sim1.25$) are semiconductors.[20] It is considered that the band structures of $(RS)_xVS_2$ and $(RS)_xTaS_2$ are similar within a simple rigid band consideration. Therefore, carriers should remain in the RS and VS_2 layers because of the nonstoichiometric composition between RS and VS_2. The fact that $(RS)_xVS_2$ is a semiconductor intensively suggests that carriers on both the VS_2 and RS layers are localized by the effect of the lattice incommensurability, contrary to the $(RS)_xTaS_2$ system. The difference in the conduction between TaS_2 and VS_2 is related to the narrow V $3d$ conduction band.

The system $(RS)_xTS_x$ (T=Ta, Nb, V) is a good example for the study of the electronic state in the quasiperiodic potential. The irrational ratio ω of the lattice constants between RS and TS_2 sublattices varies from 1.77 to 1.61 by changing the rare-earth element, so that we can treat the electronic structures with various types of quasiperiodic potentials in actual materials. It should

be noted that ω in the above compounds includes the specific number $\omega_F=(\sqrt{5}+1)/2=1.618\,03\ldots$. If an electronic system has a quasiperiodic potential with the irrational number of ω_F, the system can be treated as the Fibonacci lattice, where the wave functions and the energy spectrum are obtained analytically.[27] Therefore, $(RS)_xTS_2$ will provide knowledge for the problem of the quasiperiodic electronic system experimentally.

ACKNOWLEDGMENTS

This work was supported in part by a Grant-in-Aid 04242103 for Scientific Research from the Ministry of Education, Science and Culture, and in part by the Nissan Foundation on the Scientific Research, and the Asahi Glass Scientific Foundation.

[1]G. A. Wiegers, A. Meetsma, S. van Smaalen, R. J. Haange, J. Wulff, T. Zeinstra, J. L. de Boer, S. Kuypers, G. van Tendeloo, J. Van Landuyt, S. Amelinckx, A. Meerschaut, P. Rabu, and J. Rouxel, Solid State Commun. **70**, 409 (1989).

[2]G. A. Wiegers and A. Meerschaut, Mater. Sci. Forum. **100&101**, 101 (1991).

[3]K. Suzuki, T. Enoki, and K. Imaeda, Solid State Commun. **78**, 73 (1991).

[4]K. Suzuki and T. Enoki, Mater. Sci. Forum **91-93**, 396 (1992).

[5]A. Jayaraman, V. Narayanamurti, E. Bucher, and R. G. Meines, Phys. Rev. Lett. **25**, 368 (1970).

[6]G. A. Wiegers, A. Meetsma, R. J. Haange, and J. L. de Boer, J. Less-Common Met. **168**, 347 (1991).

[7]O. Pena, P. Rabu, and A. Meerschaut, J. Phys. Condens. Matter **3**, 9929 (1991).

[8]J. M. Zeiman, *Principle of the Theory of Solids* (Cambridge University Press, Cambridge, 1972).

[9]D. Reefman, J. Baak, H. B. Brom, and G. A. Wiegers, Solid State Commun. **75**, 47 (1990).

[10]G. A. Wiegers and R. J. Haange, J. Phys. Condens. Matter **2**, 455 (1990).

[11]J. Wulff, A. Meetsma, S. van Smaalen, R. J. Haange, J. L. de Boer, and G. A. Wiegers, J. Solid State Chem. **84**, 118 (1990).

[12]M. Kasaya, J. M. Tarascon, and J. Etourneau, Solid State Commun. **33**, 1005 (1980).

[13]K. Suzuki (unpublished).

[14]L. F. Mattheiss, Phys. Rev. B **8**, 3719 (1973).

[15]K. Sugihara, Phys. Rev. B **29**, 5872 (1984).

[16]The reflectivity of $(SmS)_{1.19}TaS_2$ was measured preliminarily. By fitting the data to the Drude-Lorentzian model, the plasma frequency is estimated at $\omega_p=1.12$ eV, corresponding to the Fermi energy $E_F=0.54$ eV.

[17]U. Walter, J. Phys. Chem. Solids **45**, 401 (1984).

[18]F. U. Hillebrecht and F. C. Fuggle, Phys. Rev. B **25**, 3550 (1982).

[19]G. Ertl and J. Kuppers, *Low Energy Electrons and Surface Chemistry* (Verlag Chemie, Weinheim, 1974).

[20]T. Kondo, K. Suzuki, and T. Enoki, Solid State Commun. **84**, 999 (1992).

[21]J. Rouxel, in *Intercalated Layered Materials,* edited by F. A. Levy (Riedel, Dordrecht, 1979), p. 229.

[22]S. J. Cho, Phys. Rev. B **1**, 4589 (1970).

[23]S. Kuypers, J. Van Landuyt, and S. Amelinckx, J. Solid State Chem. **86**, 212 (1990). The authors assured us that the in-plane electron diffraction pattern of $(SmS)_{1.19}TaS_2$ is identical to that figured in this reference.

[24]S. Aubry and G. André, Ann. Isr. Phys. Soc. **3**, 133 (1980).

[25]D. R. Hofstadter, Phys. Rev. Lett. **51**, 1198 (1983).

[26]M. Kohmoto, L. P. Kadanoff, and C. Tang, Phys. Rev. Lett. **50**, 1870 (1983).

[27]S. Ostlund and R. Pandit, Phys. Rev. B **29**, 1394 (1984).